Progress in Oceanography 197 (2021) 102619

Contents lists available at ScienceDirect

Progress in Oceanography

journal homepage: www.elsevier.com/locate/pocean

A strong summer intrusion of the Kuroshio and residence time in the northern South China Sea revealed by radium isotopes

Guizhi Wang [a,b,c,*], Shengyao Sun [a,c], Ehui Tan [a], Liwen Chen [a], Lifang Wang [a], Tao Huang [a], Kuanbo Zhou [a], Weifang Chen [a], Xianghui Guo [a]

[a] State Key Laboratory of Marine Environmental Science and College of Ocean and Earth Sciences, Xiamen University, Xiamen, China
[b] Fujian Provincial Key Laboratory for Coastal Ecology and Environmental Studies, Xiamen University, Xiamen, China
[c] Dongshan Swire Marine Station, Xiamen University, Xiamen, China

ARTICLE INFO

Keywords:
Kuroshio intrusion
Residence time
Radium isotopes
Summer
The northern South China Sea

ABSTRACT

The Kuroshio intrusion through the Luzon Strait into the northern South China Sea (SCS) is an important contributor to the heat and salt budgets of the SCS and is usually the strongest in winter. The extent of the intrusion in summer and the residence time of the very surface layer (0–5 m) in the northern SCS slope and basin areas, however, are seldom quantitatively evaluated. In this study we investigated surface distributions of radium isotopes (^{226}Ra and ^{228}Ra) across the Luzon Strait into the northern SCS in late spring to mid-summer to reveal the fraction of the Kuroshio water and the transport path of the Kuroshio intrusion in the northern SCS. The activity of ^{228}Ra ranged from 0.67 to 23.5 dpm 100 L^{-1}, with the maximum occurring at the lowest salinity of 28.8 on the northern SCS shelf and the minimum appearing east of the Luzon Strait characteristic of the more saline Ra-depleted Kuroshio water. The activity of ^{226}Ra showed a similar pattern in a smaller range of 4.63–9.64 dpm 100 L^{-1}. Distributions of ^{226}Ra and ^{228}Ra, combined with the distribution of salinity, demonstrate that three water masses contribute to the surface seawater in the northern SCS, the Kuroshio surface water, the plume water, and the island-influenced surface water. We quantified the fraction of the Kuroshio water in the northern SCS, considering the conservation of ^{226}Ra and salinity, to be in the range of 4 ± 7%–51 ± 4% with an average of 23 ± 11%. The fraction decreased southward and westward from the northwest off the Luzon Strait. The intrusion of the Kuroshio reached as far west as 115° E and as far south as 14° N. The residence time of the very surface water in the northern SCS slope and basin areas was estimated using ^{228}Ra as a timer to be 0.22 ± 0.59–9.98 ± 0.54 years with an average of 2.92 ± 2.20 years.

1. Introduction

The South China Sea (SCS), a large marginal sea, is connected with the western Pacific via the Luzon Strait, where the Kuroshio intrudes into the northern SCS. The surface Kuroshio intrusion path differs among the leaping, looping, and leaking path (Fig. 1) from one time to another, with the leaking path occurring most frequently, which is a direct flow from the northeast Luzon Strait to the southwest off Taiwan followed by a westward flow on the continental slope in the northern SCS (Yuan et al. 2006; Nan et al., 2011a,b). The Kuroshio is characterized by relatively high temperature and salinity and extremely low nutrients so that the Kuroshio intrusion contributes to the heat and salt budgets in the SCS and influences nutrient inventory in the SCS (Fang et al. 2009; Wang et al. 2012; Du et al. 2013). The Kuroshio intrusion is stronger in winter than in the other seasons in response to the reversing seasonal monsoon as revealed by temperature and salinity distributions (Shaw 1991; Qu et al. 2000). The intrusion extends up to west of 112° E in winter (Hsin et al. 2012). In summer, however, the Kuroshio current mostly leaps across the Luzon Strait (Nan 2012). Strong Kuroshio intrusion is seldom observed in summer.

Residence time is an important parameter in understanding how soon a water mass is replaced and how fast materials are transported (Pilson 2013). Using a box model of Cd, the residence time in the SCS was estimated to range from 0.2 years in the top layer (0–100 m) to 6100 years in the bottom layer (850–3500 m) (Yang et al. 2012). Liu and Gan (2017) investigated the residence time of the intrusive northwestern Pacific water through the Luzon Strait in response to the time-dependent three-dimensional basin circulation in the SCS using a

* Corresponding author at: State Key Laboratory of Marine Environmental Science, Xiamen University, Xiamen 361102, China.
E-mail address: gzhwang@xmu.edu.cn (G. Wang).

https://doi.org/10.1016/j.pocean.2021.102619
Received 5 November 2019; Received in revised form 17 March 2021; Accepted 28 May 2021
Available online 4 June 2021

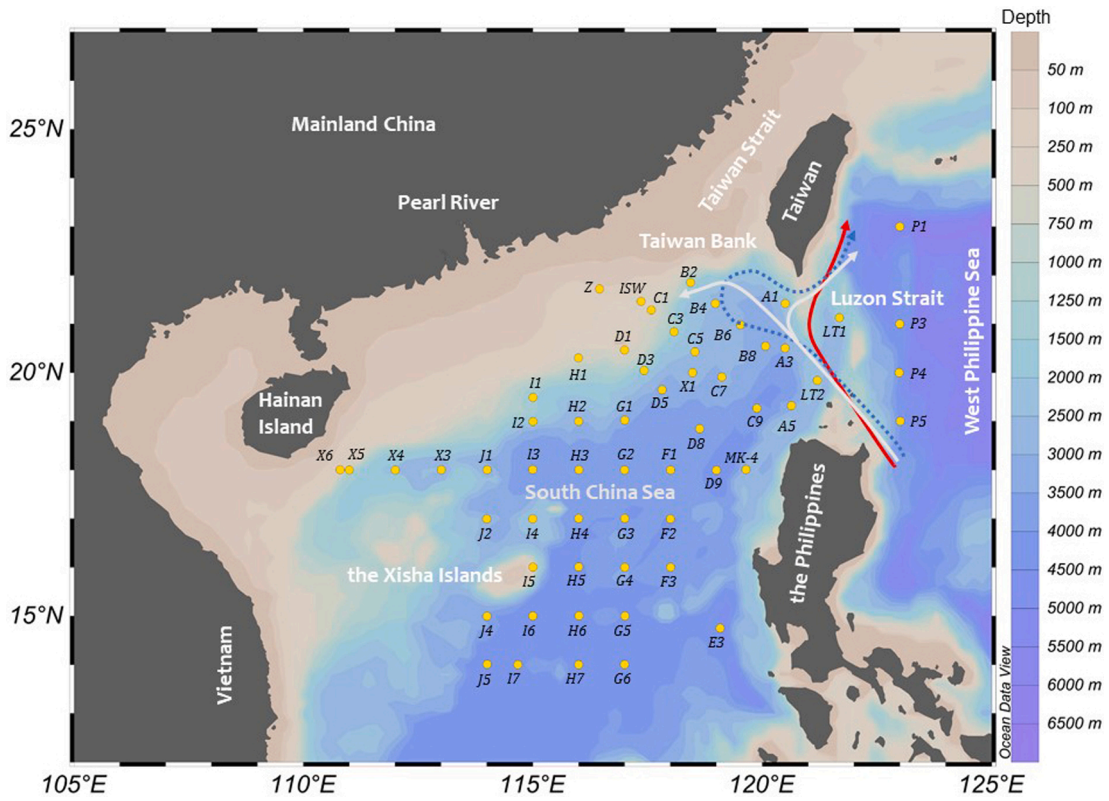

Fig. 1. Study area and sampling stations. The red, white, and dotted blue lines indicate the leaping, leaking, and looping intrusion path of the Kuroshio, respectively (Nan et al., 2011a).

numerical Eulerian analysis. Based on their study the upper (0–750 m) intrusive waters have a residence time of about 3 years on average and the deep (greater than 1500 m) intrusive waters stay in the northern SCS basin for about 25 years before subduction. However, a more focused study on the very surface layer (0–5 m) is still missing in terms of the spatial pattern of residence time in the northern SCS.

To define the extent of the Kuroshio intrusion, hydrographic parameters have been the main tools, including, but not limited to, salinity, temperature, and sea surface height from observations or numerical ocean models outputs, however, debates remain on the advantages and disadvantages of using these hydrographic tools (Nan et al. 2015). For example, salinity is a good tracer to quantify the Kuroshio intrusion since the maximum salinity of the Kuroshio water is notably higher than the SCS water (e.g., Qu et al. 2000; Yu et al. 2013). However, historical observational salinity data in the Luzon Strait area are barely available. Modeled salinity often deviates from the observational value (e.g., Nan et al. 2011a). Thus, a long-term index based on salinity cannot be established to quantify the strength of the Kuroshio intrusion (Nan et al. 2015). Long-term sea surface temperature is readily available from satellite and the Kuroshio water usually has higher temperature than the SCS water. However, the temperature difference between the Kuroshio and the SCS surface water decreases in summer due to significant warming of the SCS water, which makes it hard to distinguish the two water masses (Farris and Wimbush 1996). In addition, satellite derived sea surface temperature is often limited by cloud (Su et al. 2010). Thus, in this study, we utilized radiotracers, long-lived radium isotopes, ^{226}Ra and ^{228}Ra, to trace the Kuroshio intrusion into the northern SCS.

Naturally occurring radium isotopes are decay daughters of thorium isotopes. In contrast to their particle-reactive parents, radium isotopes readily desorb into dissolved phase in seawater. The half-life of ^{226}Ra and ^{228}Ra is 1600 years and 5.75 years, respectively, so that these two isotopes are often referred to as long-lived Ra. Away from coasts and sediments, the activity of radium in the ocean is mainly affected by mixing and decay. For example, an exponential decrease of ^{228}Ra away from the Baja California was observed in the northeast Pacific due to mixing and decay, which was used to trace eddy mixing at the length scale of 200 to 1000 km (Huh and Ku, 1998). Different water masses are generally characterized by different radium signals. River plumes are relatively enriched in Ra compared to the ambient ocean water and the Kuroshio water is depleted in Ra (Nozaki et al. 1989; Moore and Shaw 2008; Chen et al. 2010). The activity ratio of the long-lived Ra, $(^{228}Ra/^{226}Ra)_{A.R.}$, has served well as a tracer of water mass mixing in slope and basin areas where the mixing time scales are on the order of a few to tens of years (Nozaki et al. 1989) when the decay of ^{228}Ra is greater than the measurement error. In the open ocean the activity of long-lived Ra may change due to scavenging of Ra from the surface water by biogenic particles and release from the particles due to remineralization as demonstrated by significant positive correlations between the activity of ^{226}Ra and the concentration of silicate in the surface water in ocean gyres (e.g., Chung and Craig 1980; Yang et al. 2007).

The goals of this study are to show a strong summer Kuroshio intrusion, to quantity the fraction of the Kuroshio water, and for the first time ever to estimate the residence time for the very surface water in the northern SCS using chemical tracers, ^{226}Ra and ^{228}Ra, supplemented with temperature and salinity. The distributions of surface ^{226}Ra and ^{228}Ra were investigated, therefore, on both sides of the Luzon Strait and in the northern SCS slope and basin. These data haven't been published before in any other study.

2. Materials and methods

2.1. Study area

The SCS is a semi-enclosed marginal sea in the western Pacific, extending from the Tropic of Cancer to the equator. It connects with the

Table 1
Observational data in the Luzon Strait and the northern SCS. WD is the water depth. SSS is the sea surface salinity. SST is the sea surface temperature. The measurement error is listed for ^{226}Ra and ^{228}Ra.

Station	Longitude (E)	Latitude (N)	WD (m)	SSS	SST (°C)	^{226}Ra	^{228}Ra	$(^{228}Ra/^{226}Ra)_{A.R.}$	SiO_3^{2-} (μM)
						(dpm 100 L^{-1})			
P1	122.9990	22.9981	5035	34.78	27.67	5.80 ± 0.15	6.30 ± 0.32	1.09 ± 0.06	0.87
P3	123.0013	20.9992	5410	34.80	29.63	6.36 ± 0.05	1.34 ± 0.05	0.21 ± 0.01	0.74
LT1	121.6834	21.1307	2730	34.85	28.79	6.47 ± 0.08	0.79 ± 0.05	0.12 ± 0.01	0.74
P4	122.9857	19.9999	5193	34.95	29.56	5.43 ± 0.04	0.67 ± 0.03	0.12 ± 0.01	0.67
P5	123.0087	19.0032	4657	34.60	30.68	6.26 ± 0.08	0.80 ± 0.05	0.13 ± 0.01	0.81
LT2	121.1988	19.8396	3200	34.65	28.96	4.63 ± 0.07	1.21 ± 0.07	0.26 ± 0.02	0.91
A5	120.6373	19.3236	2770	33.71	31.54	7.29 ± 0.08	12.8 ± 0.21	1.76 ± 0.03	1.83
C9	119.8824	19.2698	4187	33.64	31.08	7.46 ± 0.14	13.7 ± 0.30	1.84 ± 0.05	1.57
C7	119.1228	19.9101	3257	33.99	30.43	6.88 ± 0.06	9.71 ± 0.16	1.41 ± 0.03	1.56
C5	118.5345	20.4282	2870	34.00	31.46	7.06 ± 0.08	10.8 ± 0.18	1.53 ± 0.03	1.45
C3	118.0796	20.8398	2088	33.86	30.38	7.57 ± 0.15	12.5 ± 0.35	1.65 ± 0.06	1.50
C1	117.5831	21.2847	646	33.75	29.89	7.30 ± 0.10	11.3 ± 0.24	1.55 ± 0.04	1.57
Z	116.4546	21.7185	127	28.79	30.51	9.64 ± 0.15	23.5 ± 0.44	2.43 ± 0.06	nd*
ISW	117.3596	21.4635	352	32.32	30.14	8.53 ± 0.17	15.7 ± 0.40	1.84 ± 0.06	BDL**
B2	118.4378	21.8506	1870	33.83	30.62	6.49 ± 0.10	11.2 ± 0.22	1.72 ± 0.04	1.50
B4	118.9787	21.4177	2889	33.84	30.19	7.54 ± 0.09	10.1 ± 0.17	1.35 ± 0.03	1.28
B6	119.5271	20.9809	3077	34.20	29.80	6.83 ± 0.07	5.35 ± 0.12	0.78 ± 0.02	1.22
B8	120.0745	20.5428	3670	34.19	29.65	6.84 ± 0.09	5.59 ± 0.15	0.82 ± 0.02	0.98
A3	120.4990	20.5024	2163	33.67	29.35	7.51 ± 0.12	9.38 ± 0.23	1.25 ± 0.04	1.50
A1	120.5058	21.4170	1685	34.27	28.74	6.57 ± 0.07	3.46 ± 0.10	0.53 ± 0.02	0.99
D3	117.4285	20.0463	2094	33.95	29.10	7.19 ± 0.11	8.48 ± 0.22	1.18 ± 0.04	1.55
D1	117.0003	20.4651	623	33.96	27.34	7.49 ± 0.13	8.18 ± 0.23	1.09 ± 0.04	2.08
H1	115.9982	20.3035	757	33.51	27.80	7.61 ± 0.13	9.82 ± 0.27	1.29 ± 0.04	1.25
I1	115.0071	19.4924	1570	33.31	29.26	7.36 ± 0.09	10.1 ± 0.19	1.37 ± 0.03	0.86
I2	115.0090	18.9967	2345	33.42	29.46	7.76 ± 0.14	11.1 ± 0.30	1.44 ± 0.05	0.97
H2	116.0013	19.0000	3084	33.08	29.44	7.85 ± 0.13	10.8 ± 0.27	1.38 ± 0.04	0.58
G1	117.0060	19.0211	3735	33.53	29.54	7.47 ± 0.16	10.4 ± 0.32	1.39 ± 0.05	1.27
D5	117.8212	19.6480	3145	33.59	28.71	7.53 ± 0.10	9.70 ± 0.24	1.29 ± 0.04	1.40
X1	118.4831	19.9994	2874	33.52	28.96	7.40 ± 0.14	8.96 ± 0.27	1.21 ± 0.04	1.46
M−K4	119.6473	18.0100	2785	33.25	29.01	8.45 ± 0.17	14.4 ± 0.37	1.70 ± 0.06	nd*
D9	119.0034	17.9976	4100	33.26	29.31	8.45 ± 0.13	13.1 ± 0.29	1.55 ± 0.04	1.16
D8	118.6394	18.8485	3801	33.35	29.26	7.64 ± 0.15	9.18 ± 0.29	1.20 ± 0.04	1.00
F1	118.0059	18.0012	3892	33.37	29.38	7.33 ± 0.15	12.4 ± 0.34	1.69 ± 0.06	1.28
G2	117.0024	18.0014	3937	33.29	29.52	7.58 ± 0.09	10.3 ± 0.17	1.36 ± 0.03	0.98
H3	116.0065	18.0039	3854	33.39	29.62	7.55 ± 0.09	9.56 ± 0.17	1.27 ± 0.03	nd*
I3	114.9986	18.0094	3711	33.11	29.47	7.14 ± 0.12	10.3 ± 0.24	1.44 ± 0.04	0.51
J1	114.0103	18.0038	3239	33.47	30.58	8.26 ± 0.09	20.1 ± 0.25	2.43 ± 0.04	1.19
X3	113.0069	18.0059	2095	33.32	30.68	7.80 ± 0.19	20.1 ± 0.49	2.57 ± 0.09	2.04
X4	112.0033	18.0004	2447	33.48	30.47	8.07 ± 0.12	18.6 ± 0.26	2.30 ± 0.05	1.30
X5	111.0010	17.9987	1476	33.48	30.47	8.06 ± 0.13	20.0 ± 0.41	2.48 ± 0.07	1.29
X6	110.8020	18.0056	500	33.65	30.37	7.51 ± 0.14	19.6 ± 0.40	2.61 ± 0.07	1.45
J2	113.9967	16.9984	2649	33.44	30.90	8.27 ± 0.12	20.1 ± 0.41	2.43 ± 0.06	1.15
J4	114.0019	14.9989	4250	33.40	30.23	8.39 ± 0.18	18.2 ± 0.42	2.16 ± 0.07	1.50
J5	114.0083	14.0101	4301	33.40	30.22	7.92 ± 0.15	18.1 ± 0.34	2.28 ± 0.06	1.40
I7	114.6737	14.0035	4307	33.44	29.80	8.13 ± 0.20	15.9 ± 0.43	1.95 ± 0.07	1.53
I6	114.9999	15.0025	3458	33.41	30.31	7.93 ± 0.17	17.3 ± 0.43	2.18 ± 0.07	1.50
I5	115.0087	16.0065	3100	33.37	30.02	7.66 ± 0.10	16.2 ± 0.24	2.12 ± 0.04	1.31
I4	114.9985	16.9975	2756	33.53	30.32	7.84 ± 0.18	16.4 ± 0.41	2.09 ± 0.07	1.15
H4	116.0003	17.0036	4058	33.07	30.18	7.99 ± 0.13	15.9 ± 0.36	1.99 ± 0.06	1.27
H5	116.0006	16.0105	4189	33.12	29.68	7.63 ± 0.10	15.7 ± 0.23	2.05 ± 0.04	1.29
H6	116.0058	15.0067	4165	33.30	29.95	7.90 ± 0.15	16.7 ± 0.32	2.12 ± 0.06	1.23
H7	116.0007	14.0020	4093	33.43	29.40	7.73 ± 0.18	16.3 ± 0.46	2.11 ± 0.08	1.23
G6	117.0003	14.0050	4230	32.46	29.22	7.31 ± 0.13	15.1 ± 0.31	2.07 ± 0.06	1.11
G5	117.0093	15.0012	4270	32.69	29.51	8.00 ± 0.13	16.3 ± 0.35	2.04 ± 0.05	1.15
G4	117.0050	16.0030	4111	33.22	29.75	8.09 ± 0.17	15.2 ± 0.40	1.87 ± 0.06	1.35
G3	117.0025	17.0033	4033	33.13	30.25	7.91 ± 0.10	15.6 ± 0.25	1.97 ± 0.04	1.19
F2	117.9996	16.9978	3967	33.32	30.13	8.05 ± 0.18	18.3 ± 0.53	2.27 ± 0.08	1.43
F3	118.0031	16.0026	4040	33.11	30.27	8.09 ± 0.11	15.5 ± 0.23	1.91 ± 0.04	1.20
E3	119.0849	14.7519	5105	33.13	30.22	7.21 ± 0.13	11.2 ± 0.29	1.56 ± 0.05	1.30

*nd: not determined.
**BDL: below the detection limit.

East China Sea via the Taiwan Strait in the northeast and with the western Pacific via the Luzon Strait in the east, which is the main exchange passage between the SCS and Pacific waters. Cyclonic flow along the slope forms the surface SCS circulation, which is related to the inflow transport in the upper layer in the Luzon Strait (Gan et al. 2016). The intrusion path of the Kuroshio into the SCS can change from one to another in a few weeks, with the leaking path dominant in winter and the leaping path more likely in summer (Nan et al. 2015). A weakening trend was inferred for the intrusion during the period of 1990s–2000s from observations, satellite data, and modeling results and correspondingly the mean salinity decreased in the upper water column of the northeastern SCS (Nan et al. 2015). Asian monsoon dominates the SCS, which is featured by abrupt onset of the summer southwesterly (and the monsoon rains) in mid-May and a gradual retreat for the wind direction to reverse from southwesterly to northeasterly in September–November (Wang et al. 2009). The monsoon is the main driving force of the upper

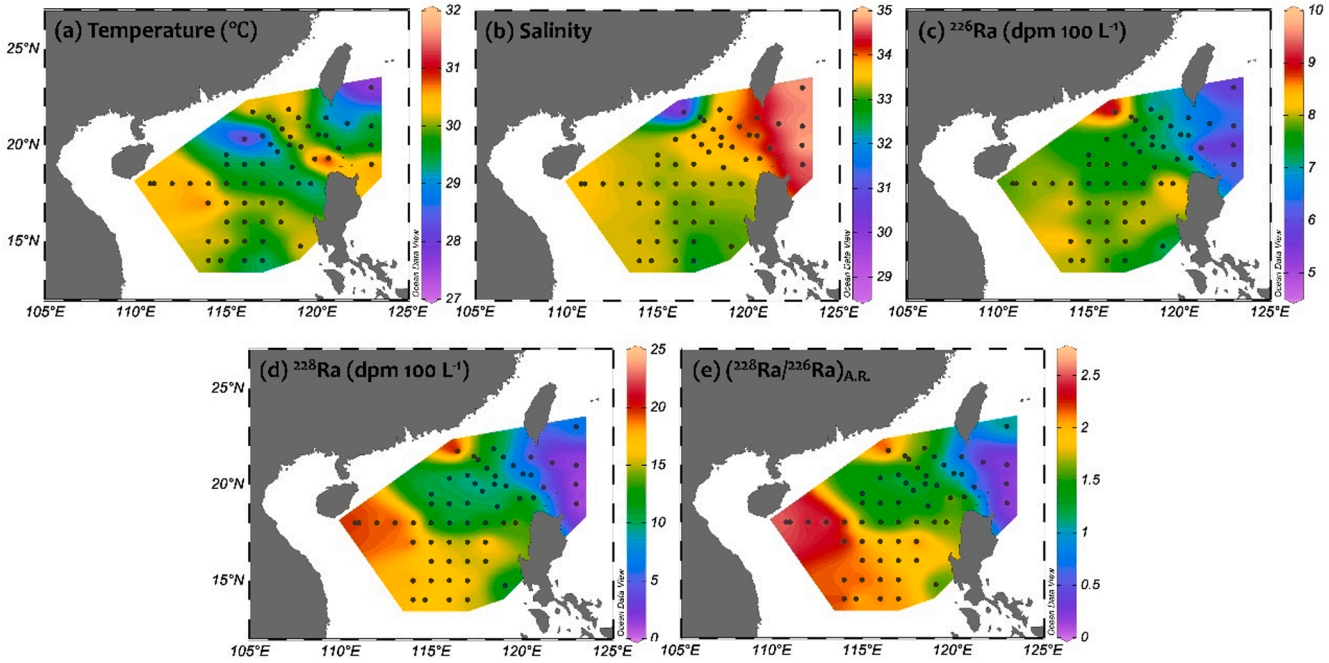

Fig. 2. Surface distributions of temperature, salinity, and long-lived Ra in the study area. (a) temperature, (b) salinity, (c) ^{226}Ra, (d) ^{228}Ra, and (e) the activity ratio of ^{228}Ra to ^{226}Ra ((^{228}Ra/^{226}Ra)$_{A.R.}$).

layer circulation of the SCS (Liu et al. 2008). A basin-scale cyclonic gyre appears in winter under northeasterly monsoon, while in summer a weak cyclonic gyre remains in the northern SCS and an anti-cyclonic gyre results in the southern SCS from the relatively weak southwesterly monsoon. Many mesoscale eddies have been observed in the SCS (Liu et al. 2008). Most of them have been found to originate in southwest of Taiwan, west of Luzon, and offshore of Central Vietnam (Wang et al. 2003). The annual mean sea surface temperature in most of the SCS ranges 26–29 °C, decreasing northward with increasing latitude and with greater temperature gradient near coasts (Zhang et al. 2017).

The Pearl River is the largest river into the northern SCS in terms of freshwater discharge and the plume water may reach east of the Taiwan Bank and even to the main channel of the Taiwan Strait when the river discharge is high and strong southwesterly winds dominate on the shelf (Bai et al. 2015; Chen et al. 2017). In the dry season the Pearl River plume flows westward under prevailing northeasterly winds (Dong et al. 2004). The annual average river discharge of the Pearl River is 3.5×10^{11} m^3 yr^{-1}, about 80% of which occurs in April–September with the remaining in October–March (Tian 1994). The Mekong River flows into the western SCS with an annual average river discharge of 4.7×10^{11} m^3 yr^{-1} (Dagg et al. 2004). The Mekong River diluted water has been found several hundred kilometers off the river mouth in the western SCS in summer (Chen et al. 2010).

2.2. Sampling and measurements

A cruise founded by the National Natural Science Foundation of China was carried out around the Luzon Strait and in the northern South China Sea during May 27–July 14, 2014 aboard *R/V Dongfanghong* II. We collected surface Ra water samples of 300–500 L from no more than 5 m below the sea surface at 60 stations using a submersible pump (Fig. 1). All the stations are located in slope and basin areas with a water depth in the range of 350–5200 m except Station Z, which is situated on the shelf at a water depth of 127 m (Table 1). The sampling time and sample volume were recorded after collection. The temperature and salinity of these samples were measured using YSI-6600D. The salinity reported here is in practical salinity scale. Dissolved Ra in these samples was extracted onboard following the procedure in Wang et al. (2015). In the lab the extracted Ra was leached and measured using an intrinsic germanium gamma detector (GCW4022 Canberra) for ^{226}Ra and ^{228}Ra as described in Moore (1984). The errors for ^{226}Ra and ^{228}Ra measurements fall in the range of 0.7–2.6% and 1.6–6.7%, respectively. The nutrient samples in the surface water were collected using a Rosette sampler at 5 m depth and analyzed onboard using a Four-channel Continuous Flow Technicon AA3 Auto-Analyzer (Bran-Luebbe, GmbH) for silicate. The detection limit for silicate was 0.05 μM.

3. Results and discussion

3.1. Surface hydrographic characteristics from the Luzon Strait to the northern SCS

The cruise started in late spring and ended in mid-summer with the cruise track from the West Philippine Sea to southeast of Taiwan Island via the Luzon Strait and further to the northern SCS shelf, slope, and basin. The spatial pattern of surface temperature in these areas is thus overlapped with the spring-summer seasonal difference. The temperature ranged from 27.3 to 31.5 °C (Table 1), with the Luzon Strait area apparently carrying the spring signal, i.e., relatively low temperature, and the western SCS having relatively high temperatures (Fig. 2a). The expected intrusion of the high-temperature Kuroshio water cannot be discerned from the temperature distribution due to the overlapping of the spatial and monthly patterns.

The salinity distribution, however, demonstrates a high-salinity tongue from the West Philippine Sea into the SCS via the Luzon Strait (Fig. 2b). The tip of the tongue reached as far west as 116° E based on salinity. The northernmost Station Z, a shelf station, had the lowest salinity, 28.79, in the study area and its closest neighbor Station ISW, a slope station, had a salinity of 32.32 (Table 1). These relatively low salinities were due to the spreading of the Pearl River plume on the northern SCS shelf toward the slope under the southwesterly monsoon and upwelling (Chen et al. 2017). Excluding Stations Z and ISW, the salinity decreased from 34.95 at Station P4 in the West Philippine Sea to 32.46 at Station G6 in the southern part of the study area. At Station G5, which is also located in the southern part of the study area and to the north of Station G6, the salinity remained low at 32.69. At other stations

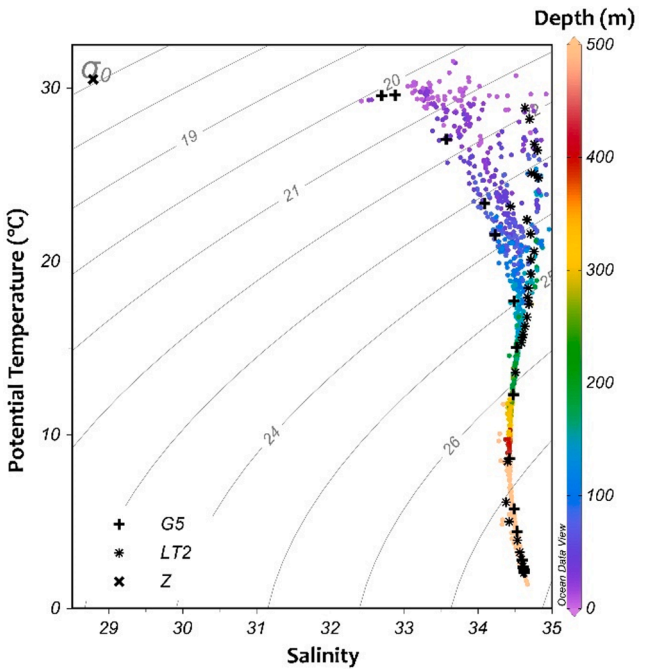

Fig. 3. Potential temperature versus salinity (T-S diagram) in the water column from the Luzon Strait to the northern SCS in May-July 2014. Data from Zhu (2015).

in the southern part of the study area, however, the salinity is no less than 33.30. This pattern indicates that a water mass with relatively low salinity must have come from the southern SCS and have spread to the southern part of the study area. Based on results in Chen et al. (2010), the Mekong River plume can travel northeastward to (114° E, 14° N). Thus, we propose based on the relatively low salinity in the southern part of the study area that the Mekong River plume travel to Station G6 (117° E, 14° N) and further to G5 (117° E, 15° N). The Kuroshio surface water had higher salinity than the plume water during the cruise period (Fig. 3).

3.2. *Surface distributions of long-lived Ra from the Luzon Strait to the northern SCS basin*

The activity of ^{226}Ra ranged from 4.63 to 9.64 dpm 100 L^{-1} in the study area, relatively low in the West Philippine Sea and the Luzon Strait and increasing westward and southward in the northern SCS (Fig. 2c). This gradual increase depicts an intrusion tongue of the Ra-depleted Kuroshio water into the SCS and subsequent mixing with the relatively Ra-replete SCS water. The peak activity occurred at the northern shelf station, Station Z, where the lowest salinity appeared due to the Pearl River plume. The relatively high activity in the western area (Stations X3-6), 7.51–8.07 dpm 100 L^{-1}, may result from terrestrial inputs from Hainan Island, most likely submarine groundwater discharge (SGD), since SGD around Hainan Island has been traced with ^{226}Ra and ^{228}Ra to be significant (Su et al. 2011; Wang et al. 2014). The relatively high activity in the southwestern areas (Stations J1, J2, J4, and J5), 7.92–8.39 dpm 100 L^{-1}, may similarly result from terrestrial inputs of SGD from the Xisha Islands considering its widespread coral reefs and reef lagoons and its similarity to other reef systems with great SGD fluxes, e.g., around the Cook Islands and Hainan Island (Tait et al. 2013; Wang et al. 2014). Sediments are not likely to be a major source of the long-lived Ra in the surface seawater in these island-influenced areas because the water depth in these areas is too deep (500–4300 m) with a mixed layer depth too shallow (17–30 m) (Jin et al. 2016) to support a diffusive transport of Ra from sediments to the sea surface high enough to result in such high activities in the sea surface. Isopycnal offshore transport of sediment-derived long-lived Ra might be present. However, we expected such source to be minor for the surface seawater although quantitative assessment was not possible for now. The minimum activity of ^{226}Ra was present at Station LT2 in the mid Luzon Strait. At Stations D9 and MK-4, which are located northwest of the Philippines, the activities of ^{226}Ra were comparable to the local maximum in the southwestern area and higher than the activities at adjacent stations, which may be due to the terrestrial influence from the Philippines with similar island-influence to those at the western and southwestern regions of the study area. SGD has been traced with Rn to be an important source of nutrients on the reef flat of Bolinao, Northwestern Philippines (Senal et al., 2011), which indicates that SGD may contribute to the relatively high Ra signal off the northwest Philippines. Their findings support our speculation of the influence of islands.

The activity of ^{228}Ra showed a similar, but more distinctive, spatial pattern to that of ^{226}Ra (Fig. 2d). The range of the activity was 0.67–23.5 dpm 100 L^{-1}, with the maximum on the northern shelf where the lowest salinity was present and the minimum in the West Philippine Sea where the highest salinity was found. The salinity and ^{228}Ra activity in the West Philippine Sea were characteristic of the high-salinity Ra-depleted Kuroshio water. The stations in the Luzon Strait carried similar high-salinity Ra-depleted signals. At Station P1, which is located east of Taiwan and northeast of the Luzon Strait, ^{228}Ra showed a relatively high signal, 6.30 dpm 100 L^{-1}, compared with the water in the Luzon Strait. One potential cause of this high ^{228}Ra was Taiwan Island. In the western and southwestern areas of the northern SCS ^{228}Ra had relatively high activities of 18.1–20.1 dpm 100 L^{-1} likely for the same reason as ^{226}Ra, i.e., terrestrial inputs, most likely SGD, from Hainan Island for the western area and from the Xisha Islands for the southwestern area. The water northwest of the Philippines (Stations D9 and MK-4) had ^{228}Ra activity of 13.1–14.4 dpm 100 L^{-1}, a few units higher compared with the adjacent waters to the west and to the north due to the influence of the Philippines although the magnitude of influence from the islands seems to be smaller in this area than in the western and southwestern areas.

The activity ratio (^{228}Ra/^{226}Ra)$_{A.R.}$ followed a spatial pattern similar to that of ^{228}Ra in the range of 0.12–2.61 (Fig. 2e). The maximum ratio appeared at the westernmost station, Station X6, which is the closest station to Hainan Island and the shallowest station near the Xisha Islands. This value is comparable to the average activity ratio, 2.8 ± 2.1, in the groundwater on the east coast of Hainan Island reported in Su et al. (2011). At the northern shelf station, which was influenced the most among all the stations by the Pearl River plume, a relatively high activity ratio of 2.43 was present. The minimum ratio was found at Station LT1, which is located in the Luzon Strait. The other stations in the Luzon Strait and east of the Strait were also characterized by relatively low activity ratios (≤0.26), comparable to the value of 0.2 in the Kuroshio water reported by Nozaki et al. (1989). This confirms that waters at these stations were from the Kuroshio. The water east of Taiwan Island at Station P1 had a relatively high activity ratio of 1.09 due to its relatively high ^{228}Ra.

3.3. *Extent of the Kuroshio intrusion and water masses in the northern SCS*

The gradual increase in Ra activity, as well as a gradual decrease in salinity, westward from the West Philippine Sea into the SCS via the Luzon Strait demonstrates an obvious intrusion path of the high-salinity Ra-depleted Kuroshio water, which intruded mainly via the northern half of the Strait, then traveled westward and mixed with the Ra-replete SCS water to as far west as 115° E (Fig. 2). West of 115° E, the Ra activity was relatively high due to Hainan Island and the Xisha Islands. This Ra-enriched water seemed to be influenced by an anticyclonic eddy that was dominant during the cruise period (Jin et al. 2016).

The above analysis of the surface distributions of salinity, ^{226}Ra, and ^{228}Ra demonstrates that four types of water masses can be distinguished in the surface water of the study area, the Kuroshio surface water (KSW),

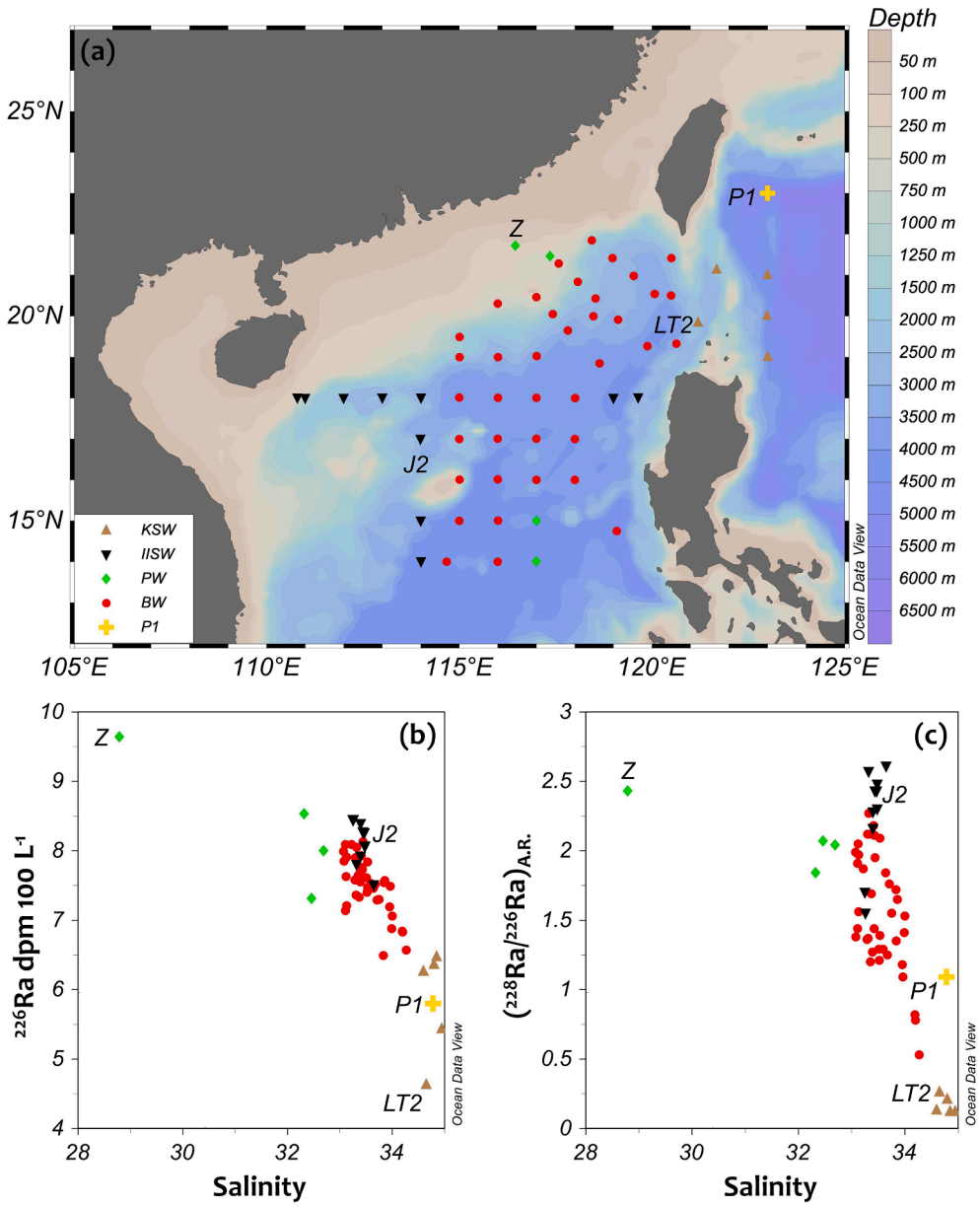

Fig. 4. Water masses in the study area and their Ra isotopic features. (a) spatial distribution of the water masses, (b) the activity of ^{226}Ra vs. salinity of these water masses, and (c) the activity ratio of ^{228}Ra to ^{226}Ra ($(^{228}Ra/^{226}Ra)_{A.R.}$) vs. salinity of these water masses.

the plume water (PW), the island-influenced surface water (IISW), and the resultant mixture of the above three water masses, i.e. the slope and basin water (BW) (Fig. 4). It has been demonstrated that mixing among different water masses was dominated by isopycnal mixing and diapycnal processes were insignificant in the upper northern SCS basin (Du et al. 2013). Taking the average diapycnal diffusivity (K_v) in the upper 40 m of the basin water in the northern South China Sea, 7.4×10^{-6} m^2 s^{-1} (Du et al. 2017), we approximated the time of vertical mixing across the pycnocline (with the length scale, L, of 100 m), $L^2/K_v = 42.9$ years, which was about seven times as much as the half-life of ^{228}Ra, so that vertical mixing can be neglected in discussing the mixing in the surface water. Here the river plume water includes the Pearl River plume in the north of the study area and the Mekong River plume in the south of the study area. KSW was characterized by the highest salinity, Ra-depletion, and the lowest $(^{228}Ra/^{226}Ra)_{A.R.}$ (Fig. 4b-c). PW was featured by the lowest salinity, Ra enrichment, and relatively high $(^{228}Ra/^{226}Ra)_{A.R.}$. IISM was also Ra enriched with relatively high $(^{228}Ra/^{226}Ra)_{A.R.}$, but its salinity was greater than that of PW. KSW, PW, and IISM were also

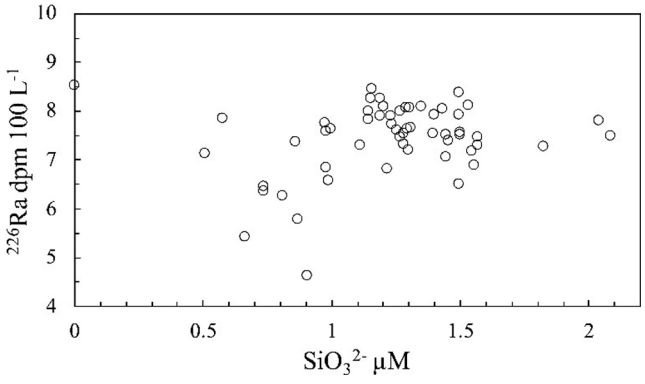

Fig. 5. The activity of ^{226}Ra vs. silicate concentration in the surface seawater in the Luzon Strait and the northern SCS slope and basin in May–July 2014.

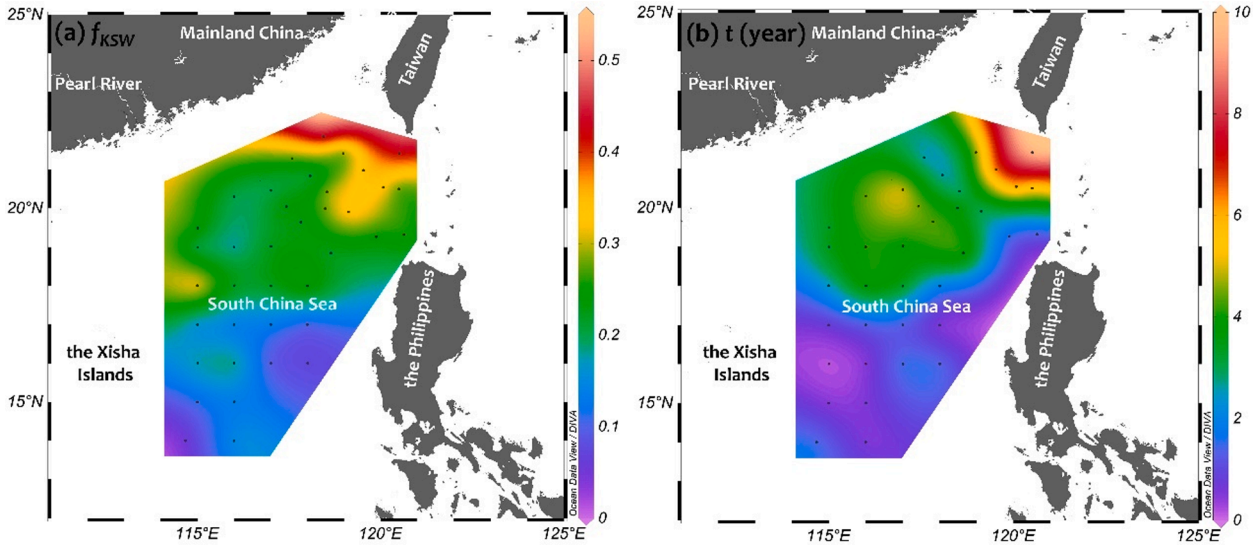

Fig. 6. Fraction of the Kuroshio water and residence time in the very surface water (0–5 m) in the northern SCS slope and basin. (a) fraction of the Kuroshio (f_{KSW}), and (b) residence time (t).

geographically separated, forming the geographic boundaries of the investigated SCS slope and basin (Fig. 4a). Station P1 is located in the West Philippine Sea northeast of the Luzon Strait. As inferred from the Kuroshio flow direction in the West Philippine Sea (Qu et al. 2000), this station had no influence on the Luzon Strait water, not to mention the SCS water. Therefore, we exclude this station in the above water mass discussion and further discussion below.

In our study region the activity of ^{226}Ra in the surface water was not significantly correlated with the concentration of silicate (Fig. 5), which suggests that the effect of biogenic particles on the Ra activity was small. ^{226}Ra, therefore, serves well as a conservative mixing tracer to estimate fractions of end-member water masses in this region. The effect of Ra removal by sinking particles would be assessed in the uncertainty analysis. The decay of ^{226}Ra is too small to measure in the northern SCS slope and basin where the residence time falls within tens of years (Liu and Gan 2017) due to its long half-life so that it can be ignored in studying oceanic processes in these areas. A three-end-member mixing model was thus set up for the slope and basin waters considering the conservation of salinity and ^{226}Ra to quantify the extent of the Kuroshio intrusion in the northern SCS,

$$\begin{cases} f_{KSW} + f_{PW} + f_{IISW} = 1 \\ S_{KSW}\cdot f_{KSW} + S_{PW}\cdot f_{PW} + S_{IISW}\cdot f_{IISW} = S_{BW} \\ {}^{226}Ra_{KSW}\cdot f_{KSW} + {}^{226}Ra_{PW}\cdot f_{PW} + {}^{226}Ra_{IISW}\cdot f_{IISW} = {}^{226}Ra_{BW} \end{cases} \quad (1),$$

where f is the fraction of each end-member in the slope and basin water, S is salinity, ^{226}Ra is the activity of dissolved ^{226}Ra, the subscript '$_{KSW}$' means the Kuroshio surface water end-member, '$_{PW}$' is the plume water end-member, '$_{IISW}$' is the island-influenced surface water end-member, S_{BW} represents the slope and basin water salinity, and $^{226}Ra_{BW}$ is the measured ^{226}Ra activity of the slope and basin water. The northern shelf Pearl River plume station, Station Z, had the lowest salinity in the study area and was taken as the PW end-member (Figs. 3-4). The activity ratio at Station Z was 2.43 ± 0.06, which is almost the same as that in the Pearl River Estuary, 2.42, at the highest salinity reported in Liu et al. (2012). This similarity in the activity ratio supports our choice of the PW end-member. The Luzon Strait station with the lowest ^{226}Ra activity, Station LT2, was taken as the KSW end-member. The activity ratio at this station was 0.26 ± 0.02, which is comparable to the value of 0.2 for the Kuroshio in Nozaki et al. (1989). This suggests that the activity ratio in the Kuroshio water stays relatively stable over the years. The island-influenced station with the highest ^{228}Ra activity, Station J2, was taken as the IISW end-member. The errors of the fractions were calculated using error propagation (Taylor 1997) considering the measurement errors of all the measured parameters in Eq. (1).

The fraction of the Kuroshio water ranged from 4 ± 7–51 ± 4% in the studied SCS slope and basin water, with an average of 23 ± 11%, decreasing southward and westward from northwest off the Luzon Strait (Fig. 6a). The maximum fraction occurred at Station B2, the northernmost slope station on the intruding path of the Kuroshio northwest of the Luzon Strait, due to its relatively low ^{226}Ra activity. The lowest fraction occurred at Station I7, the southernmost station in south of the Xisha Islands, where there was no influence of the Kuroshio water since the fraction was taken to be 0 considering its error. At Station E3, which is located at the southeastern corner of the study area, a relatively high fraction was estimated, 35 ± 5%. However, based on the decreasing southward trend of the fraction, there would be almost no influence of the Kuroshio in this region, so the estimated fraction at Station E3 was not shown in Fig. 6a to avoid misunderstanding. This overestimated fraction is due to the relatively low activity of ^{226}Ra at this station where relatively Ra-depleted southern SCS basin water (Chen et al. 2010) may play a role and scavenging by biogenic particles may likely contribute to some extent. Thus, the intrusion of the Kuroshio in the very surface water of the SCS reached as far west as 115° E and as far south as 14° N, following a general cyclonic circulation presented in Gan et al. (2016). The extent and the magnitude of the Kuroshio intrusion in the early spring to mid-summer of 2014 are seemingly greater than those in the summer of 2009 to the spring of 2011, which were station-integrated fractions over the upper 100 m estimated using an isopycnal mixing model (Du et al. 2013). Based on the results from a numerical Eulerian analysis by Liu and Gan (2017) the westward intrusion volume flux decreases with water depth for the upper 750 m in the Luzon Strait. We infer that the maximum westward intrusion occurs in the very surface layer. Therefore, the integrated fractions for the upper 100 m from the isopycnal mixing model in Du et al. (2013) are expected to be smaller than our results for the very surface layer. In addition, Du et al. (2013) estimated the Kuroshio fraction based on two water masses, the SCS proper water represented by Station SEATS (18° N, 116° E) and a typical Kuroshio water. However, in our study, the fraction of the Kuroshio was calculated based on a three end-member mixing model from the PW, IISW, and KSW water masses. The end-member of the SCS proper water from Du et al. (2013) was the basin water resulting from the mixture of the PW, IISW, and KSW water masses in our study, which would result in estimated higher Kuroshio fractions in our study. Thus, even though the

extent and magnitude of the intrusion from our study are seemingly greater than the results in Du et al. (2013), we cannot draw a conclusion that the Kuroshio intrusion in the summer of 2014 is stronger than the ones in 2009–2011.

The Kuroshio tends to leak into the SCS more frequently in winter, while it is more likely to leap across the Luzon Strait in summer (Wu and Chiang 2007). The strongest intrusion is shown to occur in winter and can reach as far as west of 112° E (Hsin et al., 2012). The probability of occurrence for leaking path in summer is just a few percent according to the compilation by Nan (2012). An intrusion in summer as strong as shown in our study (i.e., extending westward to 115° E and southward to 14° N), however, has never been demonstrated before. The mechanism driving such a strong intrusion in summer waits for physical oceanographers to step in to investigate.

The nutrient inventory of the upper 100 m water in the northern SCS slope and basin has been shown to be overall negatively correlated with the fraction of the Kuroshio water (Du et al. 2013). The air-sea CO_2 flux in the ocean-dominated margin has been suggested to be related with nutrients from the Pacific (Dai et al. 2013). Thus, it is expected that such relatively strong Kuroshio intrusion may be associated with a relatively small nutrient inventory and subsequent change in the carbon cycle in the northern SCS.

The sensitivity analysis for our mixing model was carried out in terms of the fraction of the Kuroshio water. Station I3 was taken as an example and variations in the parameters of the water masses were considered. For the PW end-member, if its salinity increased to the maximum of the water mass, 32.69, the value at Station G5, the corresponding activity of ^{226}Ra was 8.00 dpm 100 L^{-1} and the estimated fraction of the Kuroshio water at Station I3 would decrease by 33%. For the KSW end-member, an increase in the salinity to the maximum of the water mass, 34.95, the value at Station P4, would cause an increase in the calculated fraction of the Kuroshio water by 36% using the corresponding ^{226}Ra at this station. For the IISW end-member, taking the maximum and minimum salinities of the water mass, respectively with the former at Station X6 and the latter at Station X3 and using the corresponding Ra activities would result in decreases in the fraction by 33% and 25%, respectively. Besides the parameters of the end-members, a 5% increase in the activity of ^{226}Ra at Station I3 would cause a decrease in the fraction by 29%.

3.4. Residence time of the very surface water in the northern SCS

As a spatially varying local measure (Monsen et al. 2002), residence time needs a spatial distribution of a "clock" tracer to determine. The half-life of ^{228}Ra is 5.75 years, which makes it a good "clock" tracer for the surface water in the northern SCS slope and basin since the residence time of the upper intrusive water from the northwestern Pacific is approximately 3 years based on a numerical Eulerian analysis (Liu and Gan 2017). Under the assumption that the deviation of the activity of ^{228}Ra in the slope and basin water from what is derived from the mixing of the three water masses, KSW, PW, and IISW, is solely due to the decay of ^{228}Ra, we calculated the residence time of the very surface water as follows.

First, the activity of ^{228}Ra resulting from mixing of the three end-members, $^{228}Ra_{mixing}$, was calculated,

$$^{228}Ra_{Mixing} = {}^{228}Ra_{KSW}\cdot f_{KSW} + {}^{228}Ra_{PW}\cdot f_{PW} + {}^{228}Ra_{IISW}\cdot f_{IISW} \quad (2),$$

where ^{228}Ra is the activity of dissolved ^{228}Ra. The measured ^{228}Ra of the slope and basin water was expressed as

$$^{228}Ra_{BW} = {}^{228}Ra_{Mixing}\cdot exp(-\lambda_{228}\cdot t) \quad (3),$$

where λ_{228} is the decay constant of ^{228}Ra, 0.1205 year^{-1}, and t is the residence time. The residence time was then solved from Eq. (3),

$$t = \frac{1}{\lambda_{228}} ln\left(\frac{^{228}Ra_{Mixing}}{^{228}Ra_{BW}}\right) \quad (4).$$

Table 2
Salinities and radium activities of the end-members used in the mixing model and residence time calculation.

End-member	Salinity	^{228}Ra (dpm 100 L^{-1})	^{226}Ra
KSW	34.65 ± 0.05	1.21 ± 0.07	4.63 ± 0.07
PW	28.79 ± 0.05	23.4 ± 0.44	9.64 ± 0.15
IISW	33.44 ± 0.05	20.1 ± 0.41	8.27 ± 0.12

The errors of the residence time were calculated with error propagation (Taylor 1997).

The fractions of the end-members in the slope and basin water were the solution to Eq. (1). Station B2 was excluded in the residence time estimation for the following reasons. (a) This station is the northernmost slope station close to the Taiwan Bank. Besides the influences of the Kuroshio water and the plume water, it may be affected by movements of mesoscale eddies persistent in this area (Wang et al. 2003), which may carry relatively ^{228}Ra-replete shelf water to this station. (b) The ^{226}Ra activity at this station, however, is relatively low, which results in an underestimate of the fraction of the plume water and subsequent underestimate of the mixed ^{228}Ra activity simply due to mixing of the plume water, the Kuroshio water, and the island-influenced water. The observed ^{228}Ra activity at this station is, therefore, greater than the estimated mixed ^{228}Ra activity. This implies that a residence time calculation based on decay of ^{228}Ra cannot be applied for this station. With Station B2 excluded the estimated residence time of the slope and basin surface water ranged from 0.22 to 9.98 years with an average of 2.91 ± 2.20 years (Fig. 6b). This average value is similar to the residence time of the upper intrusive water into the SCS from the northwestern Pacific estimated using a numerical Eulerian analysis by Liu and Gan (2017). The residence time was longer in the northern part than in the southern part of the study area with the maximum occurring near the Luzon Strait. The interior of the basin had relatively short residence times, indicating strong mixing in this area, likely caused by mesoscale processes such as cyclonic and anticyclonic eddies commonly observed in this area (Jin et al., 2016; Nan et al., 2011b; Wang et al., 2003).

3.5. Uncertainty analysis for the residence time

From Eqs. (1, 2, 4), the total uncertainty in the residence time can result from the measurement error of every other parameter involved in these equations. Here, the uncertainty in λ_{228} is taken to be 0. The measurement errors of the end-member parameters were listed in Table 2. Using error propagation, the uncertainty in the residence time ranged from 0.4 to 0.6 years (Table 3). The major uncertainty in the residence time resulted from the measurement error of ^{226}Ra at each station, followed by the measurement error of ^{226}Ra of the IISW end-member and the measurement error of ^{228}Ra at each station. The measurement errors of the parameters of the PW and KSW end-members contributed much less to the total uncertainty, in which the measurement error of the salinity of the PW end-member contributed the least. The greater contribution of the measurement error of a parameter to the total uncertainty, the greater influence on the residence time a parameter would pose. This analysis indicates that the uncertainty in the residence time of the surface water at each slope and basin station was mainly affected by the measurement errors of the surface ^{226}Ra and ^{228}Ra activities at each station and much less affected by those of the parameters of the Kuroshio surface water and the plume water.

As for the effect of Ra removal by sinking particles, the particle flux estimated via sediment traps in the upper 374 m water column in the northern SCS is 253 mg m^{-2} d^{-1} (Yang et al. 2017). Using the average activities of ^{226}Ra and ^{228}Ra in the sinking particles in the Sargasso Sea (van Beek et al. 2007), 8.89 dpm g^{-1} and 1.19 dpm g^{-1}, respectively, the Ra due to adsorption from the surface by sinking particles in the average residence time was approximated to be 0.50 dpm ^{226}Ra 100 L^{-1} and 0.09

Table 3
Uncertainties calculated with error propagation for the residence time at each slope and basin station, including the total uncertainty and the uncertainties contributed by the measurement errors of each parameter involved in Eqs. (1, 2, 4).

Station	$\delta\_^{226}Ra_{PW}$	$\delta\_^{226}Ra_{KSW}$	$\delta\_^{226}Ra_{IISW}$	δ_S_{PW}	δ_S_{KSW}	δ_S_{IISW}	$\delta\_^{226}Ra_{BW}$	δ_S_{BW}	$\delta\_^{228}Ra_{BW}$	$\delta\_^{228}Ra_{PW}$	$\delta\_^{228}Ra_{KSW}$	$\delta\_^{228}Ra_{IISW}$	δ_total
E3	0.076	0.078	0.200	0.004	0.009	0.013	0.423	0.027	0.211	0.040	0.014	0.120	0.541
F3	0.034	0.014	0.249	0.002	0.002	0.016	0.265	0.020	0.122	0.018	0.002	0.149	0.414
F2	0.016	0.013	0.266	0.001	0.002	0.017	0.442	0.020	0.243	0.009	0.002	0.159	0.592
G3	0.039	0.024	0.243	0.002	0.003	0.016	0.245	0.021	0.134	0.021	0.004	0.145	0.401
G4	0.024	0.012	0.259	0.001	0.001	0.017	0.400	0.020	0.216	0.013	0.002	0.155	0.547
H7	0.018	0.030	0.262	0.001	0.004	0.017	0.472	0.022	0.234	0.009	0.005	0.157	0.610
H6	0.024	0.022	0.258	0.001	0.003	0.017	0.389	0.021	0.158	0.013	0.004	0.154	0.518
H5	0.053	0.043	0.226	0.003	0.005	0.015	0.277	0.023	0.122	0.028	0.008	0.135	0.409
H4	0.041	0.020	0.241	0.002	0.002	0.016	0.331	0.020	0.186	0.022	0.004	0.144	0.476
I4	0.005	0.022	0.276	0.000	0.003	0.018	0.471	0.021	0.208	0.003	0.004	0.165	0.609
I5	0.026	0.036	0.254	0.001	0.004	0.017	0.278	0.022	0.123	0.014	0.006	0.152	0.428
I6	0.013	0.018	0.269	0.001	0.002	0.018	0.417	0.020	0.208	0.007	0.003	0.161	0.563
I7	0.004	0.007	0.278	0.000	0.001	0.018	0.462	0.019	0.225	0.002	0.001	0.167	0.608
I3	0.084	0.086	0.192	0.005	0.010	0.013	0.404	0.027	0.197	0.045	0.016	0.115	0.519
H3	0.029	0.044	0.250	0.002	0.005	0.016	0.262	0.023	0.149	0.016	0.008	0.150	0.423
G2	0.038	0.043	0.242	0.002	0.005	0.016	0.254	0.023	0.140	0.020	0.008	0.145	0.410
F1	0.041	0.061	0.236	0.002	0.007	0.015	0.473	0.025	0.225	0.022	0.011	0.141	0.597
D8	0.029	0.038	0.250	0.002	0.005	0.016	0.404	0.023	0.261	0.016	0.007	0.150	0.566
X1	0.022	0.053	0.256	0.001	0.006	0.017	0.425	0.024	0.252	0.012	0.009	0.153	0.581
D5	0.010	0.041	0.269	0.001	0.005	0.018	0.285	0.023	0.208	0.005	0.007	0.161	0.475
G1	0.018	0.046	0.261	0.001	0.005	0.017	0.454	0.024	0.251	0.009	0.008	0.156	0.605
H2	0.046	0.029	0.235	0.003	0.003	0.015	0.334	0.021	0.210	0.025	0.005	0.141	0.485
I2	0.017	0.028	0.263	0.001	0.003	0.017	0.367	0.022	0.225	0.009	0.005	0.157	0.530
I1	0.046	0.060	0.231	0.003	0.007	0.015	0.279	0.025	0.152	0.025	0.011	0.138	0.425
H1	0.015	0.037	0.265	0.001	0.004	0.017	0.354	0.023	0.225	0.008	0.007	0.158	0.523
D1	0.026	0.037	0.305	0.001	0.004	0.020	0.378	0.023	0.235	0.014	0.007	0.183	0.572
D3	0.016	0.061	0.292	0.001	0.007	0.019	0.338	0.026	0.214	0.009	0.011	0.175	0.530
A1	0.037	0.120	0.306	0.002	0.014	0.020	0.292	0.032	0.247	0.020	0.022	0.184	0.540
A3	0.002	0.041	0.276	0.000	0.005	0.018	0.349	0.023	0.200	0.001	0.007	0.166	0.518
B8	0.035	0.088	0.307	0.002	0.011	0.020	0.318	0.029	0.218	0.018	0.016	0.184	0.536
B6	0.035	0.090	0.308	0.002	0.011	0.020	0.254	0.029	0.187	0.019	0.016	0.184	0.489
B4	0.015	0.036	0.294	0.001	0.004	0.019	0.250	0.023	0.137	0.008	0.006	0.176	0.449
B2	0.030	0.148	0.238	0.002	0.018	0.016	0.413	0.035	0.166	0.016	0.027	0.143	0.548
C1	0.002	0.056	0.275	0.000	0.007	0.018	0.316	0.025	0.173	0.001	0.010	0.165	0.487
C3	0.019	0.033	0.298	0.001	0.004	0.020	0.414	0.022	0.233	0.010	0.006	0.178	0.590
C5	0.019	0.071	0.294	0.001	0.008	0.019	0.253	0.027	0.137	0.010	0.013	0.176	0.455
C7	0.011	0.090	0.284	0.001	0.011	0.019	0.215	0.029	0.138	0.006	0.016	0.170	0.430
C9	0.007	0.045	0.271	0.000	0.005	0.018	0.392	0.024	0.183	0.004	0.008	0.162	0.538
A5	0.007	0.058	0.270	0.000	0.007	0.018	0.230	0.025	0.138	0.003	0.010	0.162	0.419

Note: δ_x represents the uncertainty resulting from the measurement error of x. ^{226}Ra represents the activity of ^{226}Ra. ^{228}Ra represents the activity of ^{228}Ra. S is salinity. The subscript "$_{PW}$" represents the plume water endmember, "$_{KSW}$"— the Kuroshio surface water endmember, "$_{IISW}$"— island-influenced surface water endmember, and "$_{BW}$"— the slope and basin water.

dpm ^{228}Ra 100 L^{-1}. If added to the dissolved ^{226}Ra, the residence time would increase by 63%. The amount of ^{228}Ra removed fell within the range of the measurement error, so it can be safely ignored in our calculation.

To evaluate impacts of potential variations in the values of the parameters involved in Eqs. (1, 2, 4) on the residence time, we did a sensitivity test. Station I3 was taken as an example. For the PW end-member, if the parameters at Station G5, where the maximum salinity of the PW water mass was present, were used, the residence time would decrease by 52% (Fig. 7). For the KSW end-member, using the parameter values at Station P4, where the maximum salinity of the water mass was found, would cause a decrease in the calculated residence time by 79%. For the IISW end-member, if the parameters at Station X6, which had the maximum salinity of the water mass, were used, the residence time would increase by 51%. Using the parameters at Station X3, where the minimum salinity of the water mass was found, would result in an increase in the residence time by 39%. Besides the parameters of the end-members, the variations in the activity of ^{226}Ra and ^{228}Ra at Station I3 were considered in the test. A 5% increase in the activity of ^{226}Ra at Station I3 would cause an increase in the residence time by 49% and the same percentage increase in ^{228}Ra, however, would cause a decrease in the residence time by 18%. This sensitivity test indicates that the residence time of the surface water was sensitive to the variations in the parameters of the water masses. The variation in ^{226}Ra at the sampling stations seemed to affect the residence time much more than that in ^{228}Ra.

4. Conclusions

In this study we investigated the extent and magnitude of a summer intrusion of the Kuroshio based on surface distributions of dissolved ^{226}Ra and ^{228}Ra, as well as distributions of surface temperature and salinity, from the Luzon Strait to the northern SCS in 2014. Our results present a strong Kuroshio intrusion via the Luzon Strait extending as far west as 115° E and as far south as 14° N in the northern SCS. This is the first presentation of such a strong summer intrusion of the Kuroshio. Three water masses, the Kuroshio surface water, the plume water, and the island-influenced surface water, were identified to contribute to the surface water in the northern SCS slope and basin. The fraction of the Kuroshio water averages 23 ± 11%, decreasing southward and westward from the northwest off the Luzon Strait.

The residence time of the very surface water (0–5 m) was estimated for the first time ever with observational data in the northern SCS slope and basin areas to be 2.91 ± 2.20 years on average. The residence time was longer in the northern part than in the southern part of the study area with the maximum occurring near the Luzon Strait.

Declaration of Competing Interest

The authors declare that they have no known competing financial

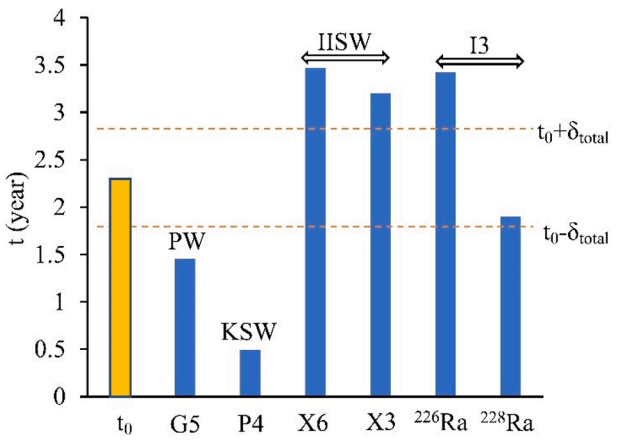

Fig. 7. Variations in the residence time (t) at Station I3 with variations in the parameters of the water masses PW, KSW, and IISW. Station G5 had the maximum salinity in the PW water mass, Station P4 had the maximum salinity in the KSW water mass, and Stations X6 and X3 had the maximum and minimum salinity, respectively in the IISW water mass. For Station I3 the left bar indicates the residence time corresponding to an increase in the activity of ^{226}Ra by 5%, and the right bar is the value corresponding to an increase in the activity of ^{228}Ra by 5%. t_0 represents the calculated residence time with the original measured parameters and δ_{total} is the uncertainty in the residence time calculated with error propagation from the measurement errors of the parameters involved in Eqs. (1, 2, 4).

interests or personal relationships that could have appeared to influence the work reported in this paper.

Acknowledgements

We thank the crew on R/V *Dongfanghong* II for their assistance in the cruise. We thank Qing Li for her logistic help before and after the cruise. We thank Chuanjun Du, Li Chen, and Yifan Zhu for silicate sample collection. We appreciate constructive comments from four anonymous reviewers that have helped to greatly improve the paper. This study was funded by MOST of PRC (2015CB954001) and the National Natural Science Foundation of China (41576074). Data and samples were collected onboard of R/V *Dongfanghong* II implementing the open research cruise NORC2014-05 supported by NSFC Shiptime Sharing Project (41349905).

Author contributions.

Guizhi Wang designed the study and wrote the article. Shengyao Sun, Ehui Tan, and Liwen Chen collected Ra samples and measured them. Lifang Wang and Tao Huang collected silicate samples and measured them. Guizhi Wang and Shenyao Sun analyzed the data. Shenyao Sun plotted the original figures in the article. Kuanbo Zhou, Weifang Chen, and Xianghui Guo guided the cruise and sample collection. All authors participated in the revision of the draft and gave the final approval of the submitted version.

References

Bai, Y., Huang, T.-H., He, X., Wang, S.-L., Hsin, Y.-C., Wu, C.-R., Zhai, W., Lui, H.-K., Chen, C.-T., 2015. Intrusion of the Pearl River plume into the main channel of the Taiwan Strait in summer. Journal of Sea Research 95, 1–15.

Chen, W., Liu, Q., Huh, C.-A., Dai, M., Miao, Y.-C., 2010. Signature of the Mekong River plume in the western South China Sea revealed by radium isotopes. Journal of Geophysical Research 115, C12002. https://doi.org/10.1029/2010JC006460.

Chen, Z., Pan, J., Jiang, Y., Lin, H., 2017. Far-reaching transport of Pearl River plume water by upwelling jet in the northeastern South China Sea. Journal of Marine Systems 173, 60–69.

Chung, Y., Craig, H., 1980. ^{226}Ra in the Pacific Ocean. Earth Planet Sci. Lett. 49 (2), 267–292.

Dagg, M., Benner, R., Lohrenz, S., Lawrence, D., 2004. Transformation of dissolved and particulate materials on continental shelves influenced by large rivers: plume processes. Cont. Shelf Res. 24 (7-8), 833–858.

Dai, M., Cao, Z., Guo, X., Zhai, W., Liu, Z., Yin, Z., Xu, Y., Gan, J., Hu, J., Du, C., 2013. Why are some marginal seas sources of atmospheric CO_2? Geophysical Research Letters 40 (10), 2154–2158.

Dong, L., Su, J., Ah Wong, L., Cao, Z., Chen, J.-C., 2004. Seasonal variation and dynamics of the Pearl River plume. Cont. Shelf Res. 24 (16), 1761–1777.

Du, C., Liu, Z., Dai, M., Kao, S.-J., Cao, Z., Zhang, Y., Huang, T., Wang, L., Li, Y., 2013. Impact of the Kuroshio intrusion on the nutrient inventory in the upper northern South China Sea: insights from an isopycnal mixing model. Biogeosciences 10 (10), 6419–6432.

Du, C.J., Liu, Z.Y., Kao, S.J., Dai, M.H., 2017. Diapycnal Fluxes of Nutrients in an Oligotrophic Oceanic Regime: The South China Sea. Geophysical Research Letters 44 (22), 11510–11518.

Fang, G., Wang, Y., Wei, Z., Fang, Y., Qiao, F., Hu, X., 2009. Interocean circulation and heat and freshwater budgets of the South China Sea based on a numerical model. Dynamics of Atmospheres and Oceans 47 (1-3), 55–72.

Farris, A., Wimbush, M., 1996. Wind-induced Kuroshio intrusion into the South China Sea. Journal of Oceanography 52 (6), 771–784.

Gan, J., Liu, Z., Liang, L., 2016. Numerical modeling of intrinsically and extrinsically forced seasonal circulation in the China Seas: A kinematic study. J. Geophys. Res. 121 (7), 4697–4715.

Hsin, Y.-C., Wu, C.-R., Chao, S.-Y., 2012. An updated examination of the Luzon Strait transport. J. Geophys. Res. 117 (C3), n/a–n/a. https://doi.org/10.1029/2011JC007714.

Huh, C.-A., Ku, T.-L., 1998. A 2-D section of 228Ra and 226Ra in the Northeast Pacific. Oceanologica Acta 21 (4), 533–542.

Jin, X., Liu, C., Poulton, A.J., Dai, M., Guo, X., 2016. Coccolithophore responses to environmental variability in the South China Sea: species composition and calcite content. Biogeosciences 13 (16), 4843–4861.

Liu, Q., Dai, M., Chen, W., Huh, C.-A., Wang, G., Li, Q., Charette, M.A., 2012. How significant is submarine groundwater discharge and its associated dissolved inorganic carbon in a river-dominated shelf system? Biogeosciences 9 (5), 1777–1795.

Liu, Q., Kaneko, A., Jilan, S.u., 2008. Recent progress in studies of the South China Sea circulation. Journal of Oceanography 64 (5), 753–762.

Liu, Z.Q., Gan, J.P., 2017. Three-dimensional pathways of water masses in the South China Sea: A modeling study. J. Geophys. Res. 122, 6039–6054. https://doi.org/10.1002/2016JC012511.

Monsen, N.E., Cloern, J.E., Lucas, L.V., 2002. A comment on the use of flushing time, residence time, and age as transport time scales. Limnol. Oceanogr. 47 (5), 1545–1553.

Moore, W.S., 1984. Radium isotope measurements using germanium detectors. Nuclear Instruments and Methods in Physics Research 223 (2-3), 407–411.

Moore, W.S., Shaw, T.J., 2008. Fluxes and behavior of radium isotopes, barium, and uranium in seven Southeastern US rivers and estuaries. Mar. Chem. 108 (3–4), 236–254.

Nan, F. 2012. Spatiotemporal Evolution of the Current-Eddy Structure Southwest of Taiwan. Ph.D. thesis, Ocean University of China, 1–119. (in Chinese with English abstract).

Nan, F., Xue, H., Chai, F., Shi, L., Shi, M., Guo, P., 2011a. Identification of different types of Kuroshio intrusion into the South China Sea. Ocean Dynamics 61 (9), 1291–1304.

Nan, F., Xue, H.J., Xiu, P., Chai, F., Shi, M.C., Guo, P.F., 2011b. Oceanic eddy formation and propagation southwest of Taiwan. J. Geophys. Res. 116, C12045. https://doi.org/10.1029/2011JC007386.

Nan, F., Xue, H., Yu, F., 2015. Kuroshio intrusion into the South China Sea: A review. Progress in Oceanography 137, 314–333.

Nozaki, Y., Kasemsupaya, V., Tsubota, H., 1989. Mean residence time of the shelf water in the East china and the Yellow seas determined by Ra-228/Ra-226 measurements. Geophysical Research Letters 16 (11), 1297–1300.

Pilson, M.E.Q., 2013. Major consituents of seawater. In: Pilson, M.E.Q. (Ed.), An introduction to the chemistry of the sea. New York, Cambridge University, Press, pp. 66–73.

Qu, T., Mitsudera, H., Yamagata, T., 2000. Intrusion of the North Pacific waters into the South China Sea. J. Geophys. Res. 105 (C3), 6415–6424.

Senal, Maria Isabel S., Jacinto, Gil S., San Diego-McGlone, Maria Lourdes, Siringan, Fernando, Zamora, Peter, Soria, Lea, Cardenas, M. Bayani, Villanoy, Cesar, Cabrera, Olivia, 2011. Nutrient inputs from submarine groundwater discharge on the Santiago reef flat, Bolinao, Northwestern Philippines. Marine Pollution Bulletin 63 (5–12), 195–200. https://doi.org/10.1016/j.marpolbul.2011.05.037.

Shaw, P.-T., 1991. The seasonal-variation of the intrusion of the philippine sea-water into the south china sea. J. Geophys. Res. 96 (C1), 821–827.

Su, F.-C., Tseng, R.-S., Ho, C.-R., Lee, Y.-H., Zheng, Q., 2010. Detecting Surface Kuroshio front in the Luzon strait from multichannel satellite data using neural networks. Geoscience and Remote Sensing Letters IEEE 7 (4), 718–722.

Su, N., Du, J., Moore, W.S., Liu, S., Zhang, J., 2011. An examination of groundwater discharge and the associated nutrient fluxes into the estuaries of eastern Hainan Island, China using 226Ra. Science of The Total Environment 409, 3909–3918.

Tait, D., Santos, I.R., Erler, D.V., Befus, K.M., Cardenas, M.B., Eyre, B.D., 2013. Estimating SGD in a South Pacific coral reef lagoon using different radioisotopes and geophysical approaches. Marine Chemistry 156, 49–60.

Taylor, J.R., 1997. An Introduction to Error Analysis. University Science Books, Sausalito.

Tian, X.P., 1994. The distribution characteristics of temperature in Lingdingyang, estuary of the Zhujiang. Tropical Oceanology 13, 76–80.

van Beek, P., Francois, R., Conte, M., Reyss, J.L., Souhaut, M., Charette, M., 2007. Ra-228/Ra-226 and Ra-226/Ba ratios to track barite formation and transport in the water column. Geochimica Et Cosmochimica Acta 71 (1), 71–86.

Wang, B., Huang, F., Wu, Z., Yang, J., Fu, X., Kikuchi, K., 2009. Multi-scale climate variability of the South China Sea monsoon: A review. Dynamics of Atmospheres and Oceans 47 (1-3), 15–37.

Wang, G.H., Su, J.L., Chu, P.C., 2003. Mesoscale eddies in the South China Sea observed with altimeter data. Geophysical Research Letters 30 (21), 2121. https://doi.org/10.1029/2003GL018532.

Wang, G., Jing, W., Wang, S., Xu, Y.i., Wang, Z., Zhang, Z., Li, Q., Dai, M., 2014. Coastal acidification induced by tidal-driven submarine groundwater discharge in a coastal coral reef system. Environmental Science and Technology 48 (22), 13069–13075.

Wang, G., Wang, Z., Zhai, W., Moore, W.S., Li, Q., Yan, X., Qi, D.i., Jiang, Y., 2015. Net subterranean estuarine export fluxes of dissolved inorganic C, N, P, Si, and total alkalinity into the Jiulong River estuary. China. Geochem. Cosmochim. Acta 149, 103–114.

Wang, X.D., Li, W., Qi, Y.Q., Han, G.J., 2012. Heat, salt and volume transports by eddies in the vicinity of the Luzon Strait. Deep-Sea Research 61, 21–33.

Wu, C.-R., Chiang, T.-L., 2007. Mesoscale eddies in the northern South China Sea. Deep-Sea Research II 54 (14-15), 1575–1588.

Yang, J., Chen, M., Qiu, Y., Li, Y., Ma, Q., Lv, E., Zhang, R., 2007. ^{226}Ra evidence for the ecosystem shift over the past 40 years in the North Pacific Substropical Gyre. Chinese Science Bulletin 52, 832–838.

Yang, J.-Y., Kao, S.-J., Dai, M., Yan, X., Lin, H.-L., 2017. Examining N cycling in the northern South China Sea from N isotopic signals in nitrate and particulate phases. Journal of Geophysical Research-Biogeosciences 122 (8), 2118–2136.

Yang, S.-C., Lee, D.-C., Ho, T.-Y., 2012. The isotopic composition of Cadmium in the water column of the South China Sea. Geochimica et Cosmochimica Acta 98, 66–77.

Yu, X., Wang, F., Wan, X., 2013. Index of Kuroshio penetrating the Luzon Strait and its preliminary application. Acta Oceanologica Sinica 32 (1), 1–11.

Yuan, D., Han, W., Hu, D., 2006. Surface Kuroshio path in the Luzon Strait area derived from satellite remote sensing data. Journal of Geophysical Research 111, C11007. https://doi.org/10.1029/2005JC003412.

Zhang, L., Ren, G., Baoleerqimuge, B.X., Yu, J., 2017. Climatology and change of the South China Sea surface temperature based on satellite observations. Climate Change Research 13 (3), 189–197.

Zhu, Y., 2015. Distribution and Dynamics of Ammonium in the South China Sea. Master thesis. Xiamen University, Xiamen, China.